International Journal of Applied and Computational Mathematics

https://www.springer.com/journal/40819

Accepted July 9th 2022

TRACER DISPERSION DUE TO PULSATILE CASSON REACTIVE FLOW IN A CIRCULAR TUBE MODULATED BY ELECTRICAL AND MAGNETIC FIELDS

D. Murugan[1], Ashis Kumar Roy[2,*] and R. Ponalagusamy[1]and O. Anwar Bég[3]

[1]Department of Mathematics, National Institute of Technology, Tiruchirappalli-620015, Tamilnadu, India.

[2]Department of Science and Humanities, Tripura Institute of Technology, Narsingarh, Tripura -799009, India.

[3]Multi-Physical Engineering Sciences Group, Mechanical Engineering Department, School of Science, Engineering and Environment (SEE), University of Salford, Manchester, M5 4WT,UK.

Abstract: The present article describes a detailed mathematical investigation of electro-magneto-hydrodynamic dispersion in the pulsatile flow of a Casson viscoplastic fluid in a tube packed with a porous medium. Using appropriate transformations, the model is rendered non-dimensional. Via the generalized dispersion method and finite Hankel transforms, analytical solutions for the solute concentration dispersion and convection coefficients have been obtained. The impact of the Hartmann (magnetic) number, Debye–Hückel (electrokinetic) parameter, Darcy number, and chemical reaction parameter with regard to dispersion phenomena has been studied. The evolution in velocity and concentration profiles are investigated graphically for realistic ranges of the various physical parameters. The present investigation, highlights the dual nature of the Debye–Hückel parameter in the dispersion process. Increment in the lower or higher magnitudes of Debye–Hückel parameter induces or decreases the magnitudes of effective dispersion coefficient, whereas it induces a reverse dual mechanism in the zenith of the average concentration profile. The present simulations are relevant to enhancing the performance of diagnostic tools in biochemical engineering, pumping of intelligent rheological working fluids in biomedicine, and also soft robotics.

Keywords: Dispersion, Casson non-Newtonian fluid, bulk-flow reaction, Hartmann number, Debye–Hückel parameter, Darcy number.

1. Introduction

The dispersion mechanism of soluble materials in fluid motion is one of the most interesting research areas in modern biomedical and industrial engineering. Taylor [1] pioneered the study of the hydrodynamics of the solute diffusion process in a tube and found that both effects of axial convection and radial molecular diffusion are significant. Aris [2] reaffirmed Taylor's methodology and

furthermore identified that the efficiency of solute diffusion in a tube is proportional to the accumulation of Taylor's dispersion coefficient and the impact of the axial molecular diffusion coefficient. Gill and Sankarasubramanian [3] proposed the generalized dispersion technique in modelling fluid flows with solute dispersion in tubes and postulated that solute dispersion characteristics could be obtained at every available point in the post-injected fluid flow regime. This method is however limited to linear and second-order differential equations. Aris's method of moment dispersion [2] was improved by Barton [4] and is known as the Aris-Barton moment method; this method guarantees a higher-order moment equation, and it is validated at every point after the injection in the dispersion mechanism. Roy et al. [5] used the Aris-Barton moment technique and finite difference implicit method to study the dispersion process in a tube.

In dispersion transport phenomena, chemical reactions may also feature which are relevant to chemical reactor systems, coagulating blood flows and hazardous waste transport. Katz [6] initiated mathematical studies of dispersion in a tube in the presence of catalytic wall chemical reactions. Subsequently, many interesting studies on reactive hydrodynamic dispersion in solute transport have been communicated, including Walker [7], Gupta and Gupta [8], Shukla et al. [9] and Kumar et al. [10], who examined the dispersion phenomenon in the channel and tubular flows with homogeneous and heterogeneous chemical reactions. These studies also addressed regular and irregular fluid motion by applying either Newtonian and non-Newtonian fluid models. Roy et al. [11] used the Aris-Barton moment technique and Hermite polynomials to study Taylor dispersion of reactive species in pulsatile viscoplastic flow in a channel with boundary absorption and bulk chemical reactions. They `noted that both chemical reactions reduce the negative exchange coefficient and the apparent dispersion coefficient, whereas they elevate the negative convection coefficient. Further, Roy and Shaw [12] analyzed the shear augmented dispersion of a solute in the microvascular mechanism by using two fluid model. They noted that increment in the yield stress and absorption parameters enhance the mean concentration profile. Das et al. [13] have investigated the solute dispersion process and influence of wall absorption parameter on a stenosed artery flow by considering Casson fluid.

Solute dispersion in non-Newtonian fluids has received increasing attention in recent years due to growing applications in bio-microfluidics. Rana and Murthy [14, 15] have applied the generalized dispersion model in pulsatile non-Newtonian (Casson [14] and Herschel-Bulkley [15]) transport in a tube with a wall reaction, motivated by computing more precisely the spreading of solute in hemodynamics. Debnath et al. [16] have investigated the solute dispersion process in three-layered pulsatile fluid motion in a tube by the Aris-Barton method. Further, Debnath et al. [17] have analyzed the solute dispersion in the Hagen-Poiseuille flow of three layer fluid in a circular tube. They observed that the convection and dispersion coefficient both decrease as the peripheral layer thickness decrease. Furthermore, Debnath et al. [18] have investigated the transport of species through an annular tube and, they pointed out that transport coefficients are linearly increased with the rate of the associated reactions but decrease with the wall absorption rate. Subsequently, Debnath et al. [19] discussed the solute

dispersion mechanism of a cylindrical pipe by considering two fluid model. They found that yield stress increases the value of dispersion coefficient decrease for all time. Recently, Chauhan and Tiwari [20] studied the combined effects of the Jeffrey fluid parameter and variable viscosity parameter on the solute dispersion process in a small blood vessels by applying generalized dispersion method. Biswas et al. [21] developed a mathematical model to endovascular drug delivery by using an image segmentation technique.

The above studies have been confined to electrically non-conducting regimes. Blood, however, is known to exhibit bioelectromagnetic characteristics owing to the presence of iron in the hemoglobin molecule in addition to the many ionic species suspended in plasma. Both electric and magnetic fields feature in many extracorporeal treatments used in physiological biomedical engineering, including drug targeting, tissue repair, relaxation therapies, etc. As such magneto-hydrodynamic flows and electrokinetic flows arise in blood flows, and indeed combined electro-magnetic flows are also present. These phenomena are accompanied by the rheological characteristics (e.g.,viscoplasticity, viscoelasticity, shear-thinning/thickening, erythrocyte microstructural spin, etc.) of streaming blood, in particular in narrow vessels and capillaries. The study of tissue electrical properties with the aid of different impedance diagnostic methods helps to scrutinize several diseases in the human body, such as cardiac dysfunction, hematological degeneration, blood coagulation mechanisms, etc. [22]. Zhao et al. [23] investigated theoretically the unsteady electro-osmotic transport in a circular tube with integral transforms and a non-Newtonian viscoelastic model. They observed that the oscillatorynature of the velocity distribution is amplifiedwith an increment in the viscoelastic fluid relaxation time parameter. Wang et al. [24] studied the electro-osmotic transport in a channel by applying Fourier transforms, noting that the electrolyte of greater level concentration slows down the electro-osmotic velocity of the microchannel. Bandopadhyay et al. [25] have examined the electrokinetic flow in the capillaries and circular pores with radial variation in viscosity due to charge-induced thickening (viscoelastic rheological behaviour), and reported that very small diameter channels along with heavy zeta potentials and constant steric effects induce the mechanism of effective viscosity. Misra et al. [26] have discussed the effects of the electro-osmotic mechanism under unsteady flow conditions in a channel using the Eringen micropolar fluid model, observing that micropolar fluid velocity, as well as microrotation gradient (wall couple stress), are elevated with greater electro-osmotic (Debye–Hückel) parameter.

As noted earlier, magnetohydrodynamics (MHD) which involves the interaction of magnetic fields and viscous or inviscid flows, arises in many clinical applications. An external applied magnetic field can be used to control human blood circulation and pressure drop. For instance, cell separation reduces the bleeding level of blood since the acting magnetic field retards blood flow. Tzirtzilakis and Loukopoulos [27] analyzed the biomagnetic flow mechanism in a channel by applying low, uniform, and high-level magnetic fields in the channel flow and obtained a numerical solution velocity field and skin friction with a finite difference method. Sarojamma and Ramana [28] observed the transport coefficients obtained by involving the generalized dispersion technique in the magnetic field on the dispersion of

Newtonian fluid through a conduit, noting that the convection coefficient is dependent on the magnetic field, whereas the exchange coefficient is acting independent of the magnetic field. Mazumdar et al. [29] have scrutinized the Newtonian fluid flow with magnetic effects in a circular tube and reported that the external applied magnetic field effectively damps the flow. Sud et al. [30] have investigated the impact of magnetic fields on blood pumping devices, noting the excellent retardation achieved.

Solute dispersion mechanisms in porous media also play a vital role in tissue engineering, especially drug fate and nutrienttransport in the lungs, brain, and kidneys, among other vessels. Porous media inhibit flow, and a relevant pathological example is blood flow impedance owing to the deposition of fatty plaques of cholesterol and artery-clogging blood clots formed in the lumen of the coronary artery. Dash et al. [31] have evaluated the velocity distribution and flow rate behaviour of Casson fluids in a tube containing a Darcianporous medium for both constant permeability and radially-varying permeability. Mehmood et al. [32] have investigated the transient axisymmetric blood transport a diseased porous arterial segment with elastic walls. They found that the pressure drop diminishes by enhancing the permeability. Hydrodynamic dispersion in porous media has also received considerable interest. Dentz et al. [33] used both asymptotic analysis and open-source finite-volume code (Open FOAM 4) to compute the dispersion in laminar flow through a 3–dimensional porous medium, defining fluid transport properties due to the pore-size distribution based on the Eulerian velocity. Shah et al. [34] studied the combined influence of heat and mass transfer on the solute dispersion mechanism in a tube with porous medium by applying the generalized dispersion method and considering two fluid model.

Inspired by these developments, the current study presents an integrated mathematical model for collective electric field and magnetic field effects on the Taylor dispersion process in pulsatile non-Newtonian blood flow (as arterial blood flow is pulsatile) through a cylindrical tube containing a porous medium with chemical reaction. Fatty plugs of cholesterol are simulated as a porous medium with Darcy's model. The novelty of the present work is, therefore, the simultaneous consideration of chemical reaction, electro-osmotic, magnetohydrodynamics, and viscoplastic pulsatile blood flow with porous medium drag. The analytical solutions of the solute concentration convection and dispersion coefficients are obtained using a generalized dispersion technique. Extensive visualization of the impact of Hartmann (magnetic) number, Debye–Hückel (electrokinetic) parameter, Darcy number and chemical reaction parameter on hydrodynamic dispersion characteristics, velocity and concentration profiles is included. The present investigation, also highlights the dual nature of the Debye–Hückel electro-osmotic parameter in the dispersion process. The current analysis may also prove beneficial in providing deeper insight into electromagnetically actuated bio-microfluidic systems as efficient solutal carriers.

2. Mathematical Formulation

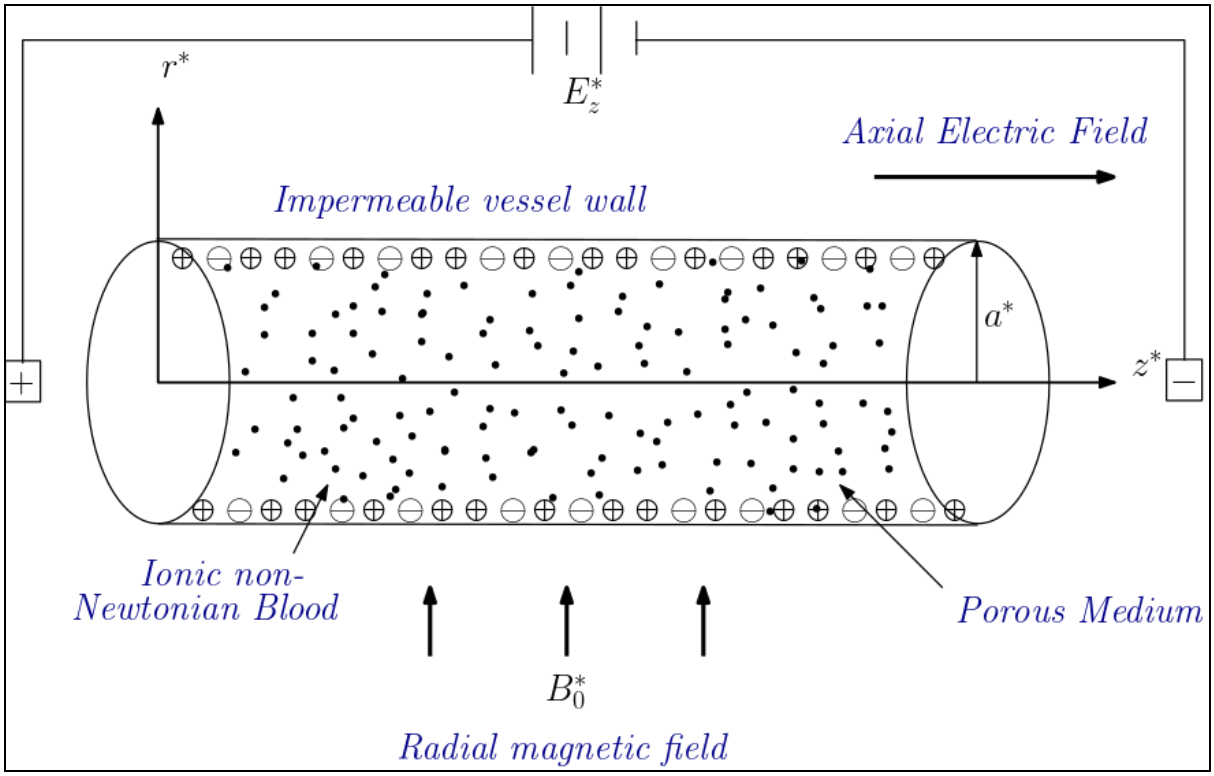

Fig.1. The geometry of the physical problem

The electro-magneto-hydrodynamic pulsatile flow of an incompressible non-Newtonian (Casson) fluid in a microtube of radius a^*, filled with a homogenous, isotropic, Darcian porous medium is considered. A cylindrical polar coordinate system is chosen, which is represented in **Fig. 1**. The variables z^* and r^* denotes the axial and radial coordinates of the system. ($*$ over a letter denotes dimensional quantity). A radial magnetic field and axial electrical field are applied. The rheological equation for the Casson fluid (electroconductive blood) is given as (Nakamura and Sawada [35], Eldabe et al. [36]):

$$\tau_{ij}^* = 2\left(\mu_c^* + P_y^* / \sqrt{2\pi}\right)e_{ij}^*, \pi^* > \pi_c^* \quad (1)$$

$$\tau_{ij}^* = 2\left(\mu_c^* + P_y^* / \sqrt{2\pi_c}\right)e_{ij}^*, \pi^* < \pi_c^* \quad (2)$$

Where $\pi^* = e_{ij}^* e_{ij}^*$ and $P_y^* = \mu_c^* \sqrt{2\pi} / \gamma$. Further, $\tau_{ij}^* = (i, j)^{\text{th}}$ is the component of the stress tensor, $e_{ij}^* = (i, j)^{\text{th}}$ represents the component of deformation rate, π^* denotes the product of the component of deformation rate with itself, π_c^* indicates the critical value of this product depends on the non-Newtonian fluid, μ_c^* is the plastic dynamic viscosity of Casson fluid, γ is the Casson parameter and

P_y^* represents the yield stress of Casson fluid. To formulate the appropriate mathematical model, the following assumptions are invoked:

1. The micro tube is filled with isotropic porous media saturated with ionic fluid (blood).

2. The boundary surface of the microtube is impermeable.

3. The fluid is ionic, electroconductive incompressible, viscoplastic blood (Casson model).

4. Fluid density (ρ^*) and kinematic viscosity (ν^*) of the Casson fluid are constant.

5. The flow mechanism is induced by periodic axial pressure gradient given as (Roy et al. [37, 38]).

6. Magnetic induction effects are negated (sufficiently low magnetic Reynolds number such that magnetic field lines are undistorted), and Hall current is omitted.

$$-\frac{1}{\rho^*}\frac{\partial p^*}{\partial z^*} = P^*\left[1+\varepsilon \,\mathrm{Re}\left(e^{i\omega^* t^*}\right)\right], \tag{3}$$

Here P^* indicates the pressure, εP^* denotes amplitude and ω^* represents the pressure pulsation frequency. Bugliarello and Sevilla [39] have emphasized that the radial velocity is vanishingly small and can be neglected for low Reynolds number hemodynamicsin microvessels (e.g.,narrow arteries). This type of flow condition is valid in small-diameter blood vessels (arterioles) and capillaries. Based on the assumptions mentioned above, the momentum equation governing the flow of electro-magnetic (ionic) Casson blood may be obtained as:

$$\frac{\partial u^*}{\partial t^*} = -\frac{1}{\rho^*}\frac{\partial p^*}{\partial z^*} + \nu^*\left(1+\frac{1}{\gamma}\right)\left[\frac{\partial^2 u^*}{\partial r^{*2}} + \frac{1}{r^*}\frac{\partial u^*}{\partial r^*}\right] - \frac{\sigma^* B_0^{*2} u^*}{\rho^*} - \frac{\nu^* u^*}{K^*} + \frac{\rho_e^* E_z^*}{\rho^*}, \tag{4}$$

Here u^* represents the axial velocity, σ^* signifies the electrical conductivity, B_0^* means the applied uniform magnetic field, K^* is the permeability of the porous medium, ρ_e^* designates the net charge density, E_z^* represents the component of uniform external electric field in the axial direction and (γ) denotes the Casson viscoplastic parameter.

Based on the Poisson-Boltzmann equation [40, 41], ρ_e^* is expressed as:

$$\rho_e^* = -\kappa\left[\frac{\partial^2 \Phi^*}{\partial r^{*2}} + \frac{1}{r^*}\frac{\partial \Phi^*}{\partial r^*} + \frac{1}{r^{*2}}\frac{\partial^2 \Phi^*}{\partial r^{*2}}\right] \tag{5}$$

Here κ is the dielectric constant and Φ^* represents the electrical potential distribution.

By adopting the Debye–Hückel approximation (see - Masliyah and Bhattacharjee [15]), the linearized

form of Eq. (5) is expressed as:

$$\beta^{*2}\Phi^{*} = \frac{\partial^2 \Phi^{*}}{\partial r^{*2}} + \frac{1}{r^{*}}\frac{\partial \Phi^{*}}{\partial r^{*}} \tag{6}$$

where β^{*} denotes the Debye–Hückel parameter, which allows for a characterization of ionic strength dependence of the activity coefficients of species in dilute aqueous solutions. The model also allows for the effect of long-range electrostatic forces among dissolved ions in the ionic blood flow. A completely miscible solute is injected into the regime and the transport equation for this solute (e.g. oxygen) in a phase averaged scale can be formulated following Zeng and Chen [42] as:

$$\frac{\partial C^{*}_{\mathbf{solute}}}{\partial t^{*}} + u^{*}(r^{*},t^{*})\frac{\partial C^{*}_{\mathbf{solute}}}{\partial z^{*}} = D_z^{*\mathbf{eff}}\frac{\partial^2 C^{*}_{\mathbf{solute}}}{\partial z^{*2}} + \frac{D_r^{*\mathbf{eff}}}{r^{*}}\frac{\partial}{\partial r^{*}}\left(r^{*}\frac{\partial C^{*}_{\mathbf{solute}}}{\partial r^{*}}\right) - \Gamma^{*}C^{*}_{\mathbf{solute}}, \tag{7}$$

with $D_z^{*\mathbf{eff}} = k(\lambda^{*} + D_z^{*}/\phi)$, $D_r^{*\mathbf{eff}} = k(\lambda^{*} + D_r^{*}/\phi)$, where D_z^{*} and D_r^{*} are the axial and transverse diffusion coefficients, respectively. λ^{*}, k and ϕ are the concentration diffusivity, tortuosity, and porosity. The initial and boundary condition for the solute transport Eq. (7) are prescribed as follows:

1. Initial condition:

$$C^{*}_{\mathbf{solute}}(0, r^{*}, z^{*}) = \frac{m\delta(z^{*})}{\phi\pi a^{*2}} \; 0 < r^{*} < a^{*} \tag{8}$$

Where m is the total mass of the injected species at the time $t^{*} = 0$.

2. Due to the impermeable boundary of the circular tube, the solute cannot penetrate the tube wall, i.e.,

$$\frac{\partial C^{*}_{\mathbf{solute}}}{\partial r^{*}} = 0 \quad \textbf{at} \quad r^{*} = a^{*}. \tag{9}$$

3. Symmetry is assumed and thus

$$\frac{\partial C^{*}_{\mathbf{solute}}}{\partial r^{*}} = 0 \quad \textbf{at} \quad r^{*} = 0. \tag{10}$$

4. As a finite quantity of solute is released in the flow field, therefore, the solute cannot be dispersed far away from the point of injection, i.e.,

$$C^{*}_{\mathbf{solute}}(t^{*}, r^{*}, \pm\infty) = 0. \tag{11}$$

3. Non-Dimensionalisation of Model

For the present problem, it is pertinent to invoke the following dimensionless quantities:

$$t = \frac{D_r^{*\mathbf{eff}}\, t^*}{a^{*2}}, \quad r = \frac{r^*}{a^*}, \quad z = \frac{z^*}{a^*}, \quad C = \frac{C^*_{\mathbf{solute}} \pi a^{*3}}{m}, \quad u = \frac{u^*}{U^*_{hs}}, \tag{12}$$

where $U^*_{hs} = -\kappa\mu^* / \Phi^*_w E^*_z$ is the Helmholtz Smoluchowski velocity (which features the axial electrical field) and Φ^*_w denotes the zeta potential on the wall of the tube.

Using Eq. (12), the momentum Eq. (4) with a given pressure gradient (Eq. (3)) is reduced to:

$$\frac{1}{\mathrm{Sc}}\frac{\partial u}{\partial t} = F\left[1 + \varepsilon Re\left(e^{i\alpha^2 \mathrm{Sc} t}\right)\right] + \left(1 + \frac{1}{\gamma}\right)\frac{1}{r}\frac{\partial}{\partial r}\left(r\frac{\partial u}{\partial r}\right) - \left(\frac{1}{\mathbf{Da}} + M^2\right)u + \beta^2\Phi, \tag{13}$$

$$\beta^2\Phi = \frac{\partial^2\Phi}{\partial r^2} + \frac{1}{r}\frac{\partial\Phi}{\partial r} \tag{14}$$

Here $\mathbf{Da} = K^* / a^{*2}$, $M = B_0^* a^* \sqrt{\sigma^* / \mu^*}$, $\alpha = a^* \sqrt{\omega / \nu^*}$, and $\mathrm{Sc} = \nu^* / D_r^{*\mathbf{eff}}$ denotes the Darcy number (dimensionless permeability), Hartmann number (ratio of Lorentz magnetic body force to viscous hydrodynamic force), Womersley number (dimensionless parameter relating pulsatile frequency to viscous force) and Schmidt number (ratio of momentum and solute species diffusivities) respectively. $F(= P^* a^{*2} / \nu^* U)$ indicates the steady component of the pressure gradient (also known as the Poiseuille number), and $F\varepsilon$ designates the amplitude of the oscillatory component of the pressure gradient, $\beta^2 = a^{*2}\beta^{*2}$ symbolizes the non-dimensional form of the electro-osmotic parameter or Debye–Hückel parameter and $\Phi = \Phi^* / \Phi^*_w$ is the dimensionless electrical potential function. The transformed boundary conditions along the tube axis (r = 0) and the wall (r = 1) emerge as:

$$u = 0 \quad \mathbf{at} \quad r = 1 \tag{15}$$

$$\frac{\partial u}{\partial r} = 0 \quad \mathbf{at} \quad r = 0 \tag{16}$$

$$\Phi = 1 \quad \mathbf{at} \quad r = 1 \tag{17}$$

$$\frac{\partial\Phi}{\partial r} = 0 \quad \mathbf{at} \quad r = 0 \tag{18}$$

In a similar fashion, the solute convective diffusive-dispersion transport equation Eq. (7) and the respective initial and boundary conditions (Eqs. (8) and (9)-(11)) can be expressed as:

$$\frac{\partial C_{\mathbf{solute}}}{\partial t} + \mathrm{Pe}\, u(r,t)\frac{\partial C_{\mathbf{solute}}}{\partial z} = \frac{1}{r}\frac{\partial}{\partial r}\left(r\frac{\partial C_{\mathbf{solute}}}{\partial r}\right) + R_D\frac{\partial^2 C_{\mathbf{solute}}}{\partial z^2} - \Gamma C_{\mathbf{solute}}, \tag{19}$$

$$C_{\mathbf{solute}}(0, r, z) = \frac{\delta(z)}{\phi}, \quad (0 < r < 1), \tag{20}$$

$$\frac{\partial C_{\mathbf{solute}}}{\partial r} = 0 \quad \mathbf{at} \quad r = 0, \tag{21}$$

$$\frac{\partial C_{\mathbf{solute}}}{\partial r} = 0 \quad \mathbf{at} \quad r = 1, \tag{22}$$

$$C_{\mathbf{solute}}(t, r, \pm\infty) = 0, \tag{23}$$

Here $\Gamma = \Gamma^* a^{*2} / D_r^{*\mathbf{eff}}$ is the reaction rate, $R_D = D_z^{*\mathbf{eff}} / D_r^{*\mathbf{eff}}$ denotes the ratio of axial and radial dispersion coefficients and $\mathrm{Pe}(= Ua^* / \phi D_r^{*\mathbf{eff}})$ is the effective Péclet number that measures the relative impact of the convection to dispersion in the saturated porous medium regime (it is also a representation of advective transport rate to mass diffusion rate).

4. Analytical Solution for the Velocity Profile

Using the boundary conditions (17) and (18), the solution of Eq. (14) is obtained as:

$$\Phi(r) = \frac{I_0(\beta r)}{I_0(\beta)}. \tag{24}$$

where I_0 denotes the first kind modified Bessel function of order zero.

Substituting Eq. (24) into Eq. (13), we get:

$$\frac{1}{\mathrm{Sc}}\frac{\partial u}{\partial t} = F\left[1 + \varepsilon\,\mathrm{Re}\left(e^{i\alpha^2 \mathrm{Sc}t}\right)\right] + \left(1 + \frac{1}{\gamma}\right)\frac{1}{r}\frac{\partial}{\partial r}\left(r\frac{\partial u}{\partial r}\right) - \left(\frac{1}{\mathbf{Da}} + M^2\right)u + \beta^2\frac{I_0(\beta r)}{I_0(\beta)} \tag{25}$$

To solve the given boundary value problem, i.e., Eqs. (15), (16) and (25), we assume a solution of the form:

$$u(r,t) = u_s + \varepsilon\,\mathrm{Re}\left(u_1 e^{i\alpha^2 \mathrm{Sc}t}\right) \tag{26}$$

Substituting Eq. (26) in Eq. (25) subject to the boundary condition (15) and (16), the following solution emerges:

$$u_s = \frac{\beta^2}{M_1^2 - N^2\beta^2}\left[\frac{I_0(\beta r)}{I_0(\beta)} - \frac{I_0(M_1 r / N)}{I_0(M_1 / N)}\right] + \frac{F}{M_1^2}\left[1 - \frac{I_0(M_1 r / N)}{I_0(M_1 / N)}\right] \tag{27}$$

$$u_1 = \frac{F}{M_1^2 + i\alpha^2}\left[1 - \frac{I_0\left(\sqrt{M_1^2 + i\alpha^2}\; r / N\right)}{I_0\left(\sqrt{M_1^2 + i\alpha^2}\; / N\right)}\right] \tag{28}$$

where $M_1^2 = \left(1/\mathbf{Da} + M^2\right)$ and $N^2 = (1 + 1/\gamma)$.

5. Generalized Dispersion Model

Following Gill [43], we can also express the species concentration in terms of average concentration $C_{\mathbf{mean}} = 2\int_0^1 rC_{\mathbf{solute}}(t,r,z)dr$ as:

$$C_{\mathbf{solute}}(t,r,z) = C_{\mathbf{mean}} + \sum_{i=0}^{\infty} g_i(r,t)\frac{\partial^i C_{\mathbf{mean}}}{\partial z^i}, \tag{29}$$

Also, the average species concentration $C_{\mathbf{mean}}$ is diffusive in nature right from the beginning, and hence, the average concentration can be expressed as follows:

$$\frac{\partial C_{\mathbf{mean}}}{\partial t} = \sum_{i=1}^{\infty} K_i(t)\frac{\partial^i C_{\mathbf{mean}}}{\partial z^i}, \tag{30}$$

The time-dependent coefficients, K_1 and K_2 in Eq. (30) are referred to as the convection and dispersion coefficient, respectively. The higher-order coefficients, K_3 and onwards are neglected (see Gill and Sankarasubramanian [44], Roy and Bég [45]) in our study. Substituting Eq. (29) into Eqns. (19) and (20), and after some algebraic simplification, we obtain the following set of partial differential equations:

$$\frac{\partial g_1}{\partial t} = \frac{1}{r}\frac{\partial}{\partial r}\left(r\frac{\partial g_1}{\partial r}\right) - \Gamma g_1 - \left(\mathrm{Pe}u + K_1\right), \tag{31}$$

$$\frac{\partial g_2}{\partial t} = \frac{1}{r}\frac{\partial}{\partial r}\left(r\frac{\partial g_2}{\partial r}\right) - \Gamma g_2 - \left(\mathrm{Pe}u + K_1\right)g_1 + (1-K_2) \tag{32}$$

$$\begin{aligned}\frac{\partial g_{k+2}}{\partial t} = \frac{1}{r}\frac{\partial}{\partial r}\left(r\frac{\partial g_{k+2}}{\partial r}\right) - \Gamma g_{k+2} - \left(\mathrm{Pe}u + K_1\right)g_{k+1} + (1-K_2)g_k \\ - \sum_{i=3}^{k+2} K_i g_{k+i-2} \quad (k = 1,2,\cdots)\end{aligned} \tag{33}$$

The initial and boundary conditions on $g_k^{'s}$ are prescribed as follows:

$$g_i(0,r) = 0, \qquad (i = 1,2,\cdots) \tag{34}$$

$$\frac{\partial g_i}{\partial r} = 0 \quad (i = 1,2,\cdots) \quad \textbf{at} \quad r = 1, \tag{35}$$

$$\frac{\partial g_i}{\partial r} = 0, \quad (i = 1,2,\cdots) \quad \textbf{at} \quad r = 0, \tag{36}$$

It follows from Eq. (29) that:

$$\int_0^1 rg_i(r,t)dr = 0 \tag{37}$$

The convection coefficient (K_1) and dipersion coefficient (K_2) can be derived as:

$$K_1(t) = -\mathrm{Pe}\,\bar{u}, \tag{38}$$

$$K_2(t) = 1 - 2\,\mathrm{Pe}\int_0^1 r g_1 u dr. \tag{39}$$

$$K_{i+2}(t) = -2\,\mathrm{Pe}\int_0^1 r g_{i+1} u dr. \tag{40}$$

Furthermore, $\bar{u}$ in Eq. (38) is the mean velocity which is defined as:

$$\bar{u} = 2\int_0^1 r u dr \tag{41}$$

With the help of Eqs. (26) and (41), we eventually obtain:

$$\begin{aligned}\bar{u} = {} & \frac{2\beta^2}{M_1^2 - N^2\beta^2}\left[\frac{I_1(\beta)}{\beta I_0(\beta)} - \frac{N I_1(M_1/N)}{M_1 I_0(M_1/N)}\right] + \frac{F}{M_1^2}\left[1 - \frac{2N I_1(M_1/N)}{M_1 I_0(M_1/N)}\right] \\ & + \varepsilon\,\mathrm{Re}\left\{\frac{F}{M_1^2 + i\alpha^2}\left[1 - \frac{2N I_1\left(\sqrt{M_1^2 + i\alpha^2}/N\right)}{\sqrt{M_1^2 + i\alpha^2}\; I_0\left(\sqrt{M_1^2 + i\alpha^2}/N\right)}\right] e^{i\alpha^2 \mathrm{Sc}\, t}\right\}\end{aligned} \tag{42}$$

5.1. Analytical Expressions for $K_1(t)$ and $K_2(t)$

To solve Eq. (31) under the initial and boundary conditions expressed in Eqs. (34)-(37), finite Hankel transforms can be deployed and these are defined as follows:

$$g_1(t; p_i) = \mathrm{H}\{g_1\} = \int_0^1 r g_1 J_0(p_i r) dr. \tag{43}$$

where J_0 is the Bessel function of order zero and p_i are the positive roots of $J_1(p_i) = 0$. The corresponding inverse transform is defined thus:

$$g_1(r,t) = \mathrm{H}^{-1}\{\tilde{g}_1(t; p_i)\} = \sum_{i=0}^{\infty} \frac{2J_0(p_i r)}{J_0^2(p_i)} \tilde{g}_1(t; p_i). \tag{44}$$

Taking the Hankel transform of Eqs. (31) and (34) with the aid of Eqs. (35) and (36) gives:

$$\frac{\partial \tilde{g}_1}{\partial t} + \left(\beta + p_i^2\right) g_1 = -I_1, \tag{45}$$

$$g_1(0; p_i) = 0. \tag{46}$$

where

$$I_1 = \mathbf{Pe}\int_0^1 r(u - \bar{u}) J_0(p_i r) dr. \tag{47}$$

The solution of Eq. (45) can be obtained using Eq. (46) as follows:

$$\tilde{g}_1(t;p_i) = -\mathbf{Pe}\left[A_i \times \frac{1-e^{-(\Gamma+p_i^2)t}}{\Gamma+p_i^2} + \varepsilon\,\mathrm{Re}\left\{ B_i \times \frac{e^{i\alpha^2\mathbf{Sc}t} - e^{-(\Gamma+p_i^2)t}}{\Gamma+p_i^2+i\alpha^2\mathbf{Sc}} \right\} \right], \tag{48}$$

$$\begin{aligned} A_i = {} & \frac{\beta^2}{M_1^2 - N^2\beta^2}\left[\frac{\beta}{\beta^2+p_i^2}\frac{I_1(\beta)}{I_0(\beta)} - \frac{M_1 N}{M_1^2+N^2p_i^2}\frac{I_1(M_1/N)}{I_0(M_1/N)} \right] J_0(p_i) \\ & - \frac{F}{M_1}\frac{N}{M_1^2+N^2p_i^2}\frac{I_1(M_1/N)}{I_0(M_1/N)} J_0(p_i) \end{aligned} \tag{49}$$

$$B_i = -\frac{F}{\sqrt{M_1^2+i\alpha^2}}\frac{N}{M_1^2+i\alpha^2+N^2p_i^2}\frac{I_1\left(\sqrt{M_1^2+i\alpha^2}/N\right)}{I_0\left(\sqrt{M_1^2+i\alpha^2}/N\right)} J_0(p_i) \tag{50}$$

Substituting Eq. (26) into Eq. (38) yields:

$$\begin{aligned} K_1(t) = -\mathrm{Pe}\Bigg[& \frac{2\beta^2}{M_1^2-N^2\beta^2}\left[\frac{I_1(\beta)}{\beta I_0(\beta)} - \frac{N I_1(M_1/N)}{M_1 I_0(M_1/N)} \right] + \\ & \frac{F}{M_1^2}\left[1 - \frac{2N I_1(M_1/N)}{M_1 I_0(M_1/N)} \right] \\ & + \frac{F\varepsilon\,\mathrm{Re}\left(e^{i\alpha^2\mathrm{Sc}t}\right)}{M_1^2+i\alpha^2}\left[1 - \frac{2N I_1\left(\sqrt{M_1^2+i\alpha^2}/N\right)}{\sqrt{M_1^2+i\alpha^2}\; I_0\left(\sqrt{M_1^2+i\alpha^2}/N\right)} \right] \Bigg] \end{aligned} \tag{51}$$

Implementing Eqs. (26) and (44) in Eq. (39), we obtain:

$$K_2(t) = R_D - 4\,\mathrm{Pe}\sum_{i=0}^{\infty}\frac{\tilde{g}_1(t;p_i)}{J_0^2(p_i)}\left\{ A_i + \varepsilon\,\mathrm{Re}\left(B_i e^{i\alpha^2\mathbf{Sc}t} \right) \right\} \tag{52}$$

5.2. Mean Concentration

To estimate the mean concentration (cross-sectional average concentration), we have recalled Eq. (30) by truncating the third term onwards from the infinite series. By solving this truncated equation with the aid of initial and boundary conditions, following Debnath et al. [46], we obtain:

$$C_{\mathbf{mean}} = \frac{1}{2\sqrt{\pi\chi(t)}}\exp\left(-\frac{\left(z-\mathbf{Pe}\,\bar{u}t\right)^2}{4\chi(t)} \right), \tag{53}$$

$$\chi(t) = \int_0^t K_2(s)ds. \tag{54}$$

6. Results and Discussion

In the present study, we have investigated the integrated effect of axially applied pressure, axial electric field, and transverse magnetic field on the solute dispersion process. To deal with the problem, we estimate the velocity distribution, dispersion coefficient, and mean concentration coefficient in terms

of the following dimensionless variables: Schmidt number $(\mathbf{Sc})$, Peclet number $(\mathbf{Pe})$, Debye–Hückel parameter (β), Darcy number $(\mathbf{Da})$, Hartmann number (M), Womersley number (α), Casson viscoplastic parameter (γ), chemical reaction parameter (Γ) and time (t). The range of these parameters are displayed in **Table 1**.

Table.1. Range of controlling parameter in the present study

Parameter	Range or values	Reference
Womersely number (α)	0, 0.5, 1, 1.5, 2	[16]
Poiseuille number (F)	1	[37]
Schmidt number $(\mathbf{Sc})$	1000	[47, 51]
Amplitude factor (ε)	0 (Steady flow), 1.5 (Unsteady flow)	[37, 47]
Darcy number $(\mathbf{Da})$	0.01, 0.1, 0.5, 1, 5, 10	[47]
Hartmann number (M)	0, 0.5, 1, 1.5, 2	[47]
Péclet number $(\mathbf{Pe})$	100	[47]
Debye–Hückel parameter (β)	0, 0.25, 0.5, 0.75, 1 (Small value), 5, 10, 100 (large value)	[23, 48]
Porosity (ϕ)	0.6, 0.75, 0.9	[47]
Bulk flow reaction rate (Γ)	0, 10, 20, 50, 100	[38, 47]

6.1. Velocity distribution

The radial distribution of the velocity at a time instance $t=1$ with various underlying parameters is shown in **Figs. 2a-c**. Figure 2a reveals that with the increase of Darcy number, velocity will increase; however, the increment rate is gradually reduced with an increase of Darcy number; this fact is also identified by Roy et. al. [47]. A higher Darcy number implies a depletion in the Darcian drag force since progressively less solid fibers arise in the medium. This accelerates the radial flow. The magnetic number, i.e., the Hartmann number, also influences the flow velocity as outlined by Fig. 2(b). It is evident that elevation in Hartmann number amplifies the Lorentz magneto-hydrodynamic drag force, which serves to damp the axial velocity i.e., induces radial flow deceleration. From Fig. 2(c), it is apparent that as the Debye–Hückel parameter (β) increases, there is a boost in the velocity, *i.e*., radial flow acceleration is induced. It is also evident that the rate of increment in velocity gradually increases with the Debye–Hückel parameter. Moreover, for the small Debye–Hückel parameter $(\beta<1)$, the flow profile is parabolic. In Fig. 2, for all plots, smooth parabolic axial velocity profiles are computed across the microtube cross-section.

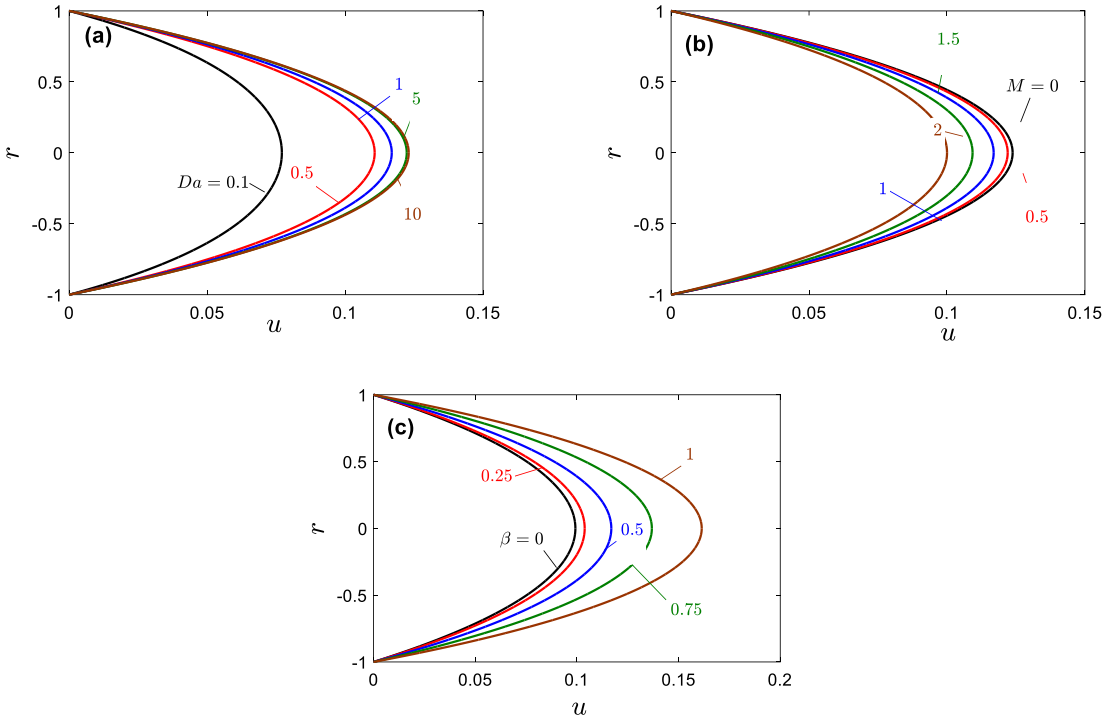

Fig. 2. Velocity distribution at time $t=1$ ($\mathbf{Sc}=1000, \varepsilon=1.5, \alpha=0.5, \gamma=0.5$) for (a) different Darcy number $(\mathbf{Da})$ and fixed $M=1, \beta=0.5$ and; (b) different Hartmann number and fixed $\mathbf{Da}=1, \beta=0.5$ (c) different Debye–Hückel parameter (β) and fixed $\mathbf{Da}=1, M=1$.

Fig. 3a-c visualize axial velocity evolution for (a) different Darcy number $(\mathbf{Da})$ with $M=1, \beta=0.5$, (b) different Hartmann number and fixed $\mathbf{Da}=1, \beta=0.5$ (c) different Debye–Hückel parameter (β) and fixed $\mathbf{Da}=1, M=1$. Inspection of the plots shows that in the absence of pressure field, the velocity gradient sharply increases at the wall vicinity for the large Debye–Hückel parameter (Fig. 3(a) and 3(c)). However, this sharp velocity gradient becomes weak in the absence of the magnetic field $(M=0)$ and will disappear with high Darcy number $\mathbf{Da}>1$ i.e., very large permeability of the porous medium (Fig. 3(c)). It is important to note that, in contrast to small Debye–Hückel parameter $\beta(<1)$ where velocity profile is nearly parabolic, the topology is morphed into plug flow in the core region, for large $\beta(\geq 5)$ and Darcy number in the absence of pressure and magnetic field $(F=0,$ **and,** $M=0)$. This result is consistent with the computations of Paul and Ng [48].

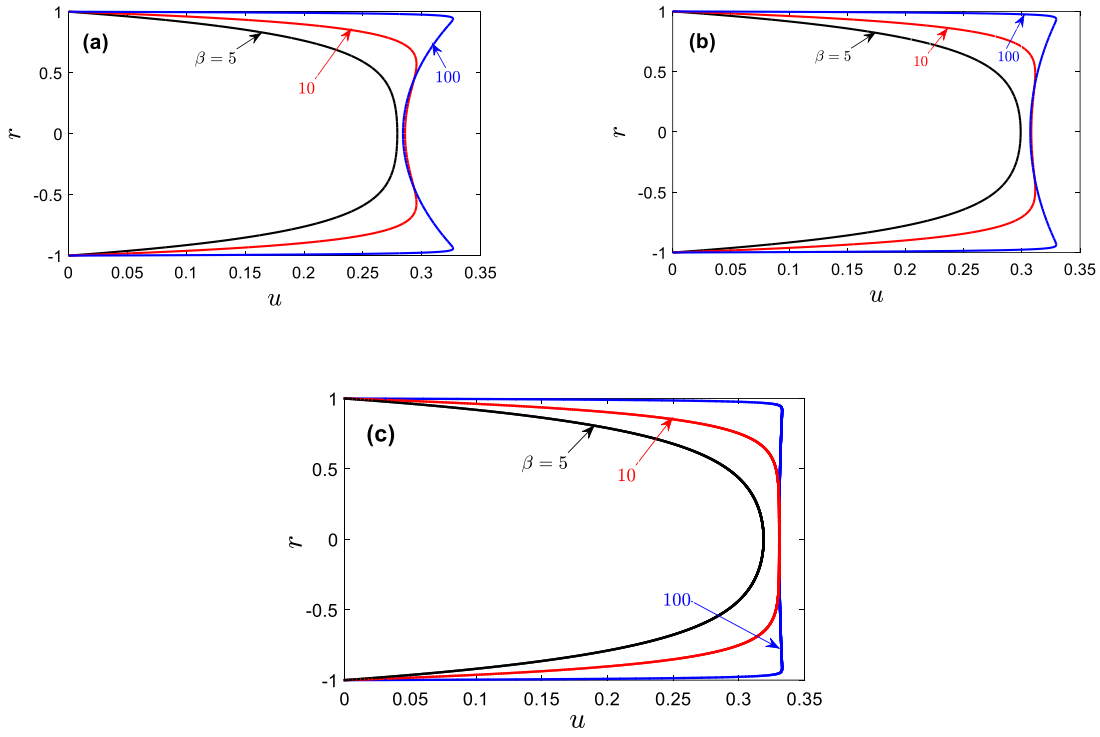

Fig. 3. Velocity distribution at time $t = 1, (\mathbf{Sc} = 1000, \varepsilon = 1.5, \gamma = 0.5, \alpha = 0.5)$ for different Debye–Hückel parameter (β), (a) without pressure field $(F = 0, M = 1, \mathbf{Da} = 1)$; (b) without pressure and magnetic field $(F = 0, M = 0, \mathbf{Da} = 1)$; (c) without pressure and magnetic field and high Darcy number $(F = 0, M = 0, \mathbf{Da} = 10)$

Figures 4a-c show the responses of axial velocity distribution for various values of Casson parameter (γ) at time t =1 for (a) without pressure field $(F = 0, M = 1, \mathbf{Da} = 1)$; (b) without pressure and magnetic field $(F = 0, M = 0, \mathbf{Da} = 1)$; and (c) without pressure and magnetic field and high Darcy number $(F = 0, M = 0, \mathbf{Da} = 10)$. In all cases, with the increase of the Casson parameter, the velocity magnitude is enhanced. As γ increases, the yield stress of the ionic viscoplastic blood decreases, which leads to an elevation in velocity, i.e., radial flow acceleration, and the effect is understandably most prominent in the core region.

6.2. Dispersion Coefficient

In this section, the effective dispersion coefficient defined by $D_E = (K_2 - R_D)/Pe^2$ is computed and illustrated. Consistent with previous studies, the current study also shows the oscillatory nature of the dispersion coefficient (see **Figs. 5, 6, 9, 11, and 12**); this is due to the pulsatile pressure gradient. The amplitude of the oscillation gradually increases and reaches its steady limit at large times, generally after $t > 0.4$. Figure 5 shows that in the absence of an electric field, i.e., $\beta = 0$, the effective dispersion coefficient decreases with increasing Hartmann number (M), which is consistent with the earlier study of Roy et al. [47]. Evidently, therefore larger transverse (radial) magnetic field suppresses

hydrodynamic dispersion in the regime. However, an increment in Darcy number (*Da*) enhances the dispersion coefficient (see Fig. 6) since a reduced porous medium impedance (Darcian linear bulk drag) is present, which permits better dispersion of the solute in the tube. Figs. 6 and 7 confirm this trend. Figure 7 indicates that the effective dispersion coefficient monotonically decreases with elevation in the Hartmann number and decays to zero for $M > 5$, which concurs with earlier investigations, including Sarojamma and Ramana [28]. The decrement of the effective dispersion coefficient is associated with the deceleration in radial flow induced by an increase in Hartmann number (average velocity decreases with stronger magnetic field). Figure 8 depicts that with an increase in Darcy number, the effective dispersion coefficient increases but eventually assumes an invariant magnitude. The increase of Darcy number enhances the permeability of the medium, which initially encourages solute dispersion, but eventually, this attains a steady behaviour.

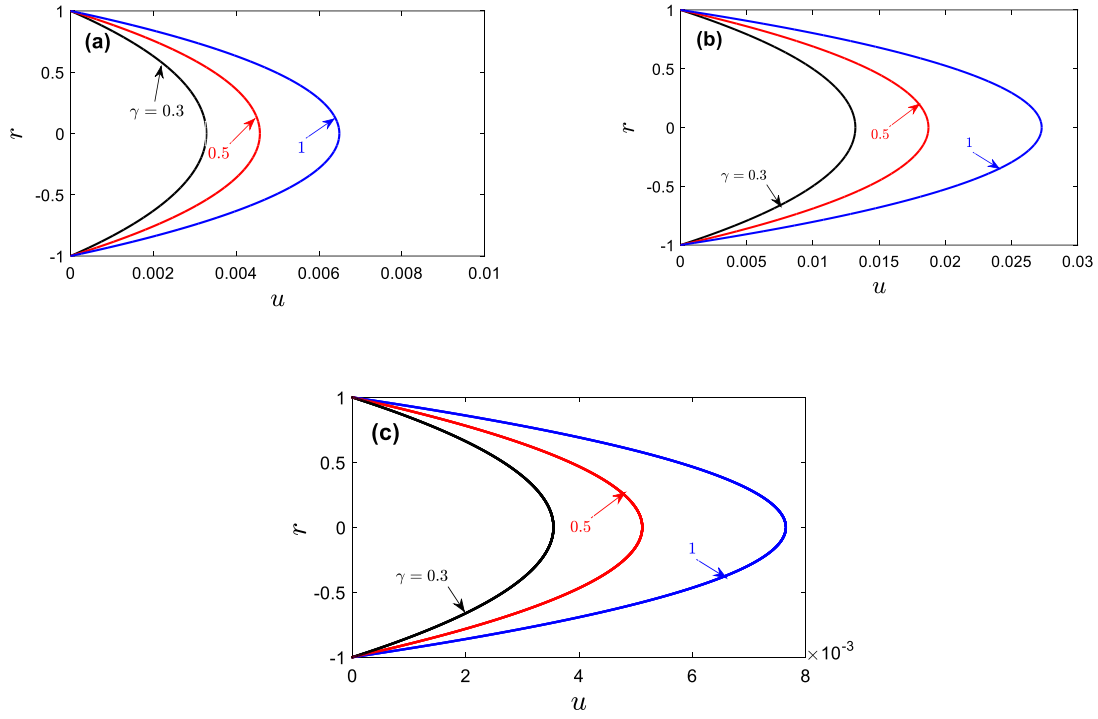

Fig. 4. Velocity distribution at time $t = 1, (\mathbf{Sc} = 1000, \varepsilon = 1.5, \beta = 0.5, \alpha = 0.5)$ for different Casson parameter (γ), (a) without pressure field $(F = 0, M = 1, \mathbf{Da} = 1)$; (b) without pressure and magnetic field $(F = 0, M = 0, \mathbf{Da} = 1)$; (c) without pressure and magnetic field and high Darcy number $(F = 0, M = 0, \mathbf{Da} = 10)$.

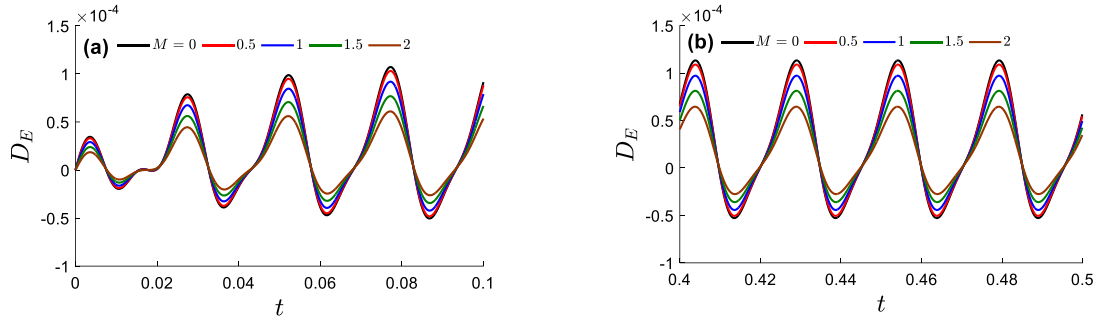

Fig. 5. Effective dispersion coefficient without electric field with (a) small and (b) large time, for different Hartmann number (M) when $F=1$, $\alpha=0.5$, $\varepsilon=1.5$, $\gamma=0.5$, $\mathbf{Sc}=1000$, $Pe=100$, $\Gamma=20$, $\mathbf{Da}=1$.

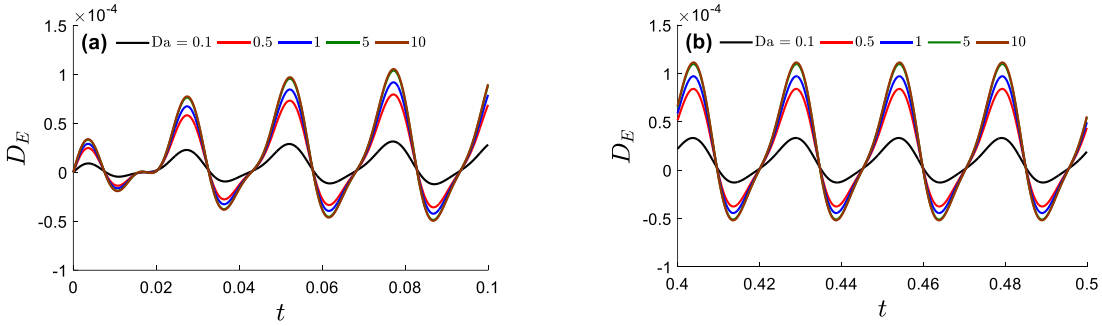

Fig. 6. Effective dispersion coefficient without electric field with (a) small and (b) large time, for different Darcy number $(\mathbf{Da})$ when $F=1$, $\alpha=0.5$, $\varepsilon=1.5$, $\gamma=0.5$, $\mathbf{Sc}=1000$, $Pe=100$, $\Gamma=20$, $M=1$.

The effective dispersion coefficient is also observed to be increased with a boost in Debye–Hückel parameter in the initial range (see Fig. 9a,b); however, for large value of Debye–Hückel parameter, this dependency assumes the opposite trend (see Fig. 9c, d). This behaviour is also captured in Fig. 10. This is attributable to the following effect- as the average velocity increases with Debye–Hückel parameter (stronger electrical axial field), this produces an initial elevation in dispersion coefficient. However, a subsequent further increase in Debye–Hückel parameter will lead to uniform velocity in the core region, which results in a depression in the dispersion coefficient. Figure 10 further elucidates that the maximum dispersion is achieved initially with increasing Debye–Hückel parameter with the lower value of Hartmann number. **Table 2** is summarizes these computations. It is important to mention here that for high Debye–Hückel parameter, the oscillatory behaviour of the effective dispersion coefficient is eliminated, i.e., stifled (see Fig. 9c, d). The influences of Casson parameter on the dispersion coefficient is depicted in Fig. 11, and it is apparent that with the increase in the Casson parameter, for all times, the dispersion coefficient is boosted. Physically, with an increase in γ, there is a reduction

in flow resistance which results in a concomitant elevation in dispersion coefficient. Figure 12 reveals that the increment in the first-order chemical reaction parameter inhibits the dispersion mechanism in the tube both for small and large time circumstances. Physically, improvement in chemical reaction parameter (Γ) leads to an increasing number of moles of solute undergo the chemical reaction and this mechanism control the solute distribution process. This result agrees with the result of Roy and Bég [45].

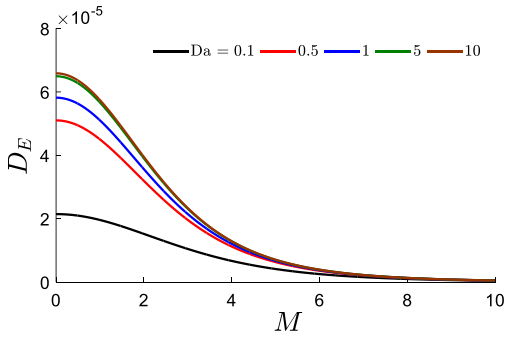

Fig. 7. Effective dispersion coefficient at time 0.5 with Hartmann number (M) for different Darcy number (**Da**) when $F=1$, $\alpha=0.5$, $\varepsilon=1.5$, $\gamma=0.5$, **Sc** $=1000$, **Pe** $=100$, $\beta=0.5$, $\Gamma=20$.

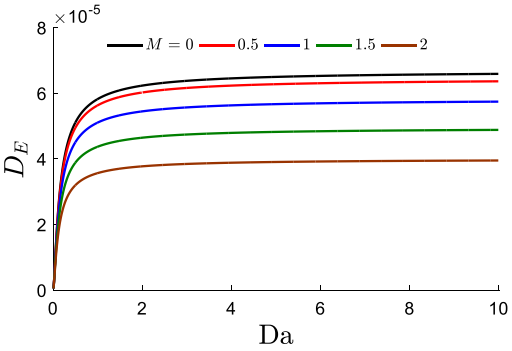

Fig. 8. Effective dispersion coefficient at time 0.5 with Darcy number (Da) for different Hartmann number (M) when $F=1$, $\alpha=0.5$, $\varepsilon=1.5$, $\gamma=0.5$, **Sc** $=1000$, **Pe** $=100$, $\beta=0.5$, $\Gamma=20$.

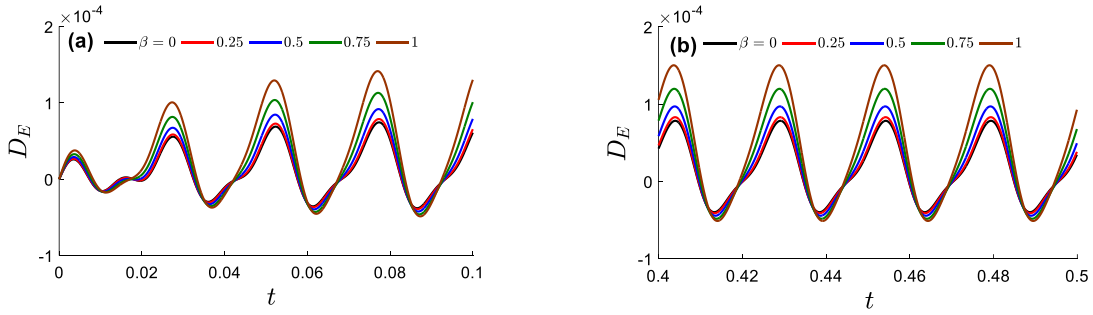

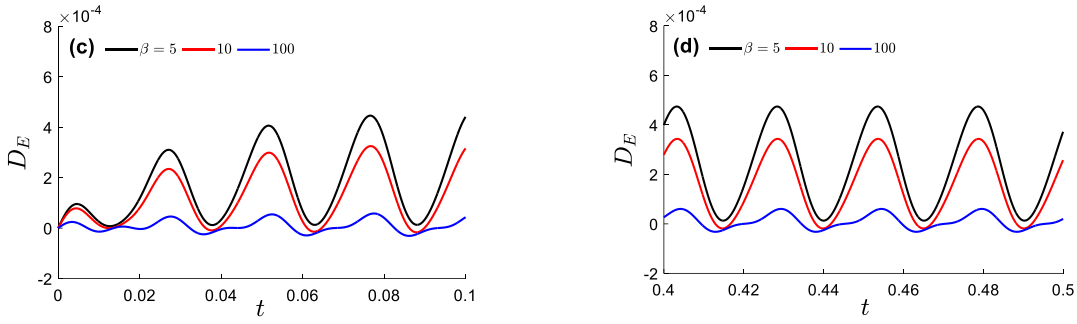

Fig. 9. Effective dispersion coefficient with (a, c) small and (b, d) large time, for different Debye–Hückel parameter (β) (small (a, b) and large (c, d)), when $F = 1$, $\alpha = 0.5$, $\gamma = 0.5$, $\varepsilon = 1.5$, $\mathbf{Sc} = 1000$, $\mathbf{Pe} = 100$, $\Gamma = 20$, $\mathbf{Da} = 1$ and $M = 1$.

Table 2 Maximum dispersion values as they appear in Fig. 9

Hartmann number	Debye–Hückel parameter	Maximum dispersion coefficient
0	4.5	4.4×10^{-4}
0.25	4.6	4.238×10^{-4}
0.5	4.4	3.787×10^{-4}
0.75	4.4	3.175×10^{-4}
1	4.3	2.52×10^{-4}

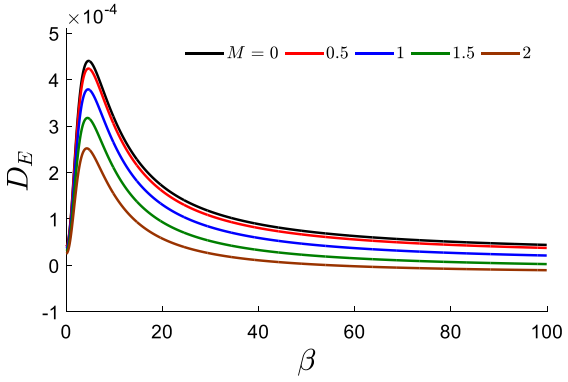

Fig. 10. Effective dispersion coefficient at time 0.5 with Debye–Hückelparameter (β) for different Hartmann number (M) when $F = 1$, $\alpha = 0.5$, $\varepsilon = 1.5$, $\gamma = 0.5$, $\mathbf{Sc} = 1000$, $\mathbf{Pe} = 100$, $\Gamma = 20$.

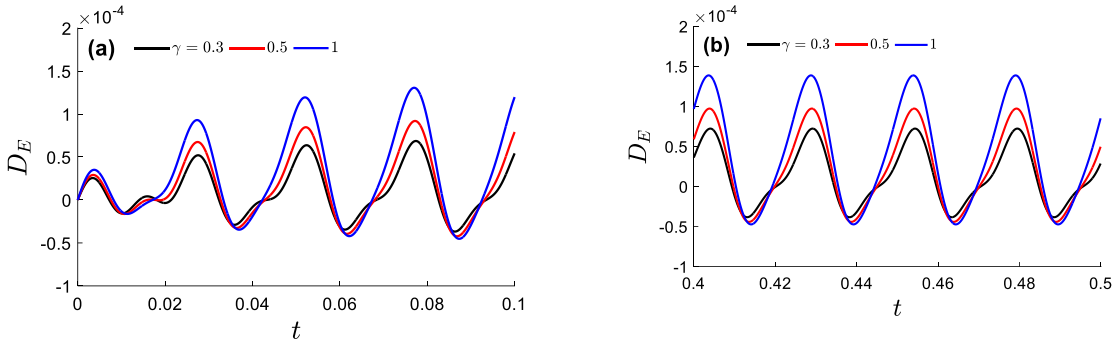

Fig. 11. Effective dispersion coefficient with (a) small and (b) large time, for different casson parameter (γ) when $F=1$, $\alpha=0.5$, $\varepsilon=1.5$, $\gamma=0.5$, **Sc**$=1000$, **Pe**$=100$, $\beta=0.5$, $M=1$, **Da**$=1$.

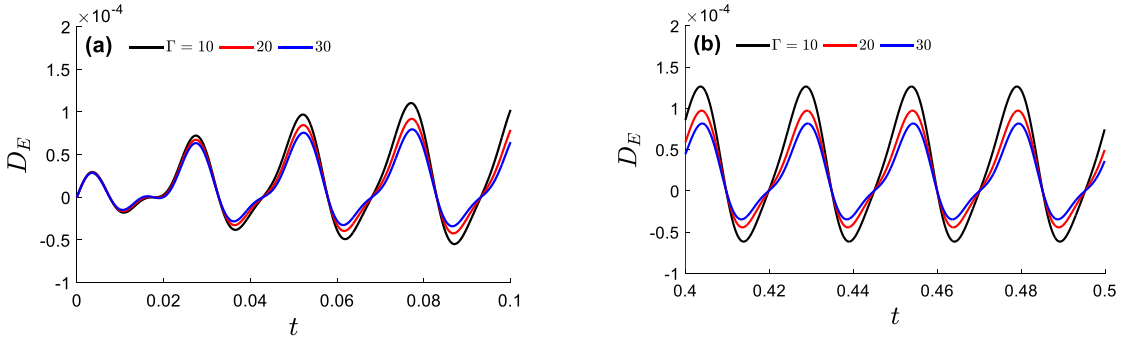

Fig. 12. Effective dispersion coefficient with (a) small and (b) large time, for different reaction parameter (Γ) when $F=1$, $\alpha=0.5$, $\varepsilon=1.5$, $\gamma=0.5$, **Sc**$=1000$, **Pe**$=100$, $\beta=0.5$, $M=1$, **Da**$=1$.

6.3. Mean concentration

Figures 13-15 illustrate the mean concentration distribution, i.e., $C_{\mathbf{mean}} \times \mathbf{Pe}$ at a time instance $t=0.5$ for various parameters. As anticipated, the profiles exhibit a Gaussian distribution symmetric about the centre of the gravity of the injected slug. Figure 13a also highlights the fact that with the increase of porosity of the medium, the peak of mean concentration is suppressed; however, an increment in chemical reaction parameter increases the peak mean concentration. These observations have also been made by Roy et al. [47].

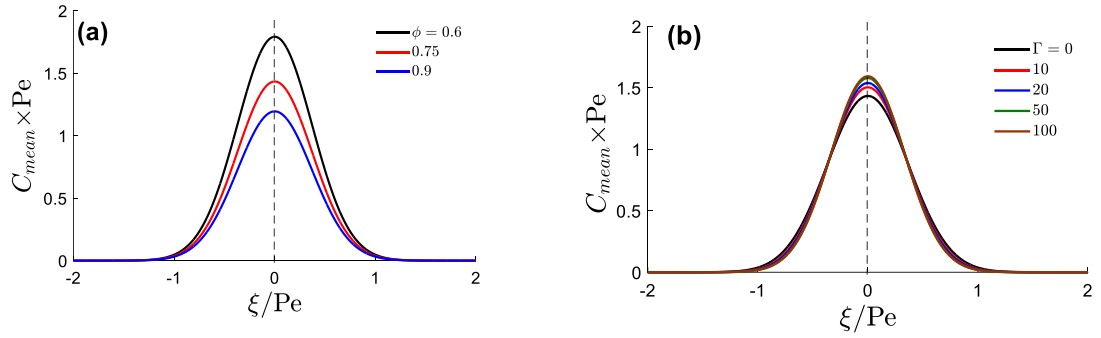

Fig. 13. Mean concentration distribution at time $t = 0.5$ (a) for various porosity (ϕ) and fixed reaction rate $\Gamma = 20$; (b) for various reaction rate (Γ) and fixed porosity $\phi = 0.75$ when $F = 1$, $\alpha = 0.5$, $\varepsilon = 1.5$, $\gamma = 0.5$, **Sc** $= 1000$, **Pe** $= 100$, $\beta = 0.5$, **Da** $= 1$, $R_D = 1$, and $M = 1$.

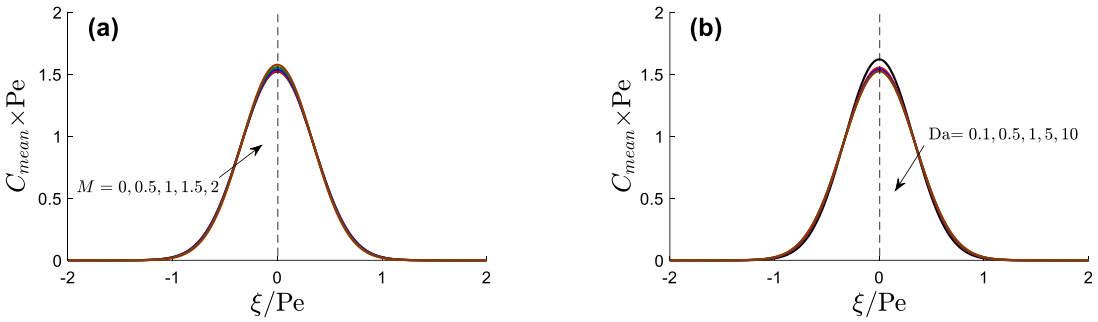

Fig. 14. Mean concentration distribution at time $t = 0.5$ (a) for different Hartmann number (M) and fixed Darcy number **Da** $= 1$; (b) for different Darcy number (**Da**) and fixed Hartmann number $M = 1$ when $F = 1$, $\alpha = 0.5$, $\varepsilon = 1.5$, $\gamma = 0.5$, **Sc** $= 1000$, **Pe** $= 100$, $\beta = 0.75$, $\Gamma = 20$ and $\phi = 0.75$.

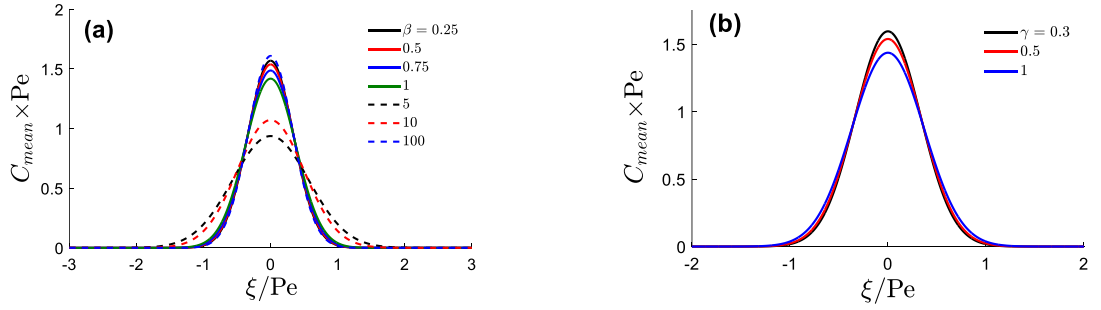

Fig. 15. Mean concentration distribution at time $t = 0.5$ (a) for different Debye–Hückel parameter (β) and fixed Casson parameter $\gamma = 0.5$; (b) for different Casson Parameter (γ) and fixed Debye–Hückelparameter $\beta = 0.5$ when $F = 1$, $\alpha = 0.5$, $\varepsilon = 1.5$, $\gamma = 0.5$, $\mathbf{Sc} = 1000$, $\mathbf{Pe} = 100$, $\beta = 0.75$, $\Gamma = 20$ and $\phi = 0.75$.

Figure 14a shows that an increase in the Hartmann number increases the peak of the Gaussian curve, whereas a rise in the Darcy number reduces the peak (Fig. 14b). This may be attributable to the modification in flow velocity with the Darcy number and Hartmann number. Figure 15a illustrates how $C_{\mathbf{mean}} \times \mathbf{Pe}$ behaves with both small and large value of Debye–Hückel parameter. Furthermore, the mean concentration also shows a dual nature with Debye–Hückel parameter. For the small value peak of the mean concentration is decreased, whereas, for the large value of this parameter, the reverse trend is computed. This has already been explained earlier. Figure 15b depicts that with the increase of the Casson parameter, the mean peak of the mean concentration is noticeably suppressed.

7. Conclusions

Motivated by developments in bionic microfluidics and smart biochemical systems, the present article has described a mathematical study of the solute dispersion in electro-magneto-hydrodynamic pulsatile ionic blood flow in a vessel (tube) containing a porous medium. The Casson viscoplastic model has been adopted, and first-order chemical reaction included. The transformed boundary value problemhas been methodically solved to derive analytical expressions for solute dispersion via a generalized dispersion method and finite Hankel transforms. A detailed parametric study of the impact of Hartmann (magnetic) number, Debye–Hückel (electrokinetic) parameter, Darcy number, and chemical reaction parameter on dispersion characteristics, velocity, and concentration profiles has been conducted. The principal findings of the simulations may be summarized as follows:

I. An enhancement in the magnitude of the Darcy number $(\mathbf{Da})$ boosts the velocity profile as well as effective dispersion coefficient (D_E) values. The amplitude of the oscillation of the effective dispersion coefficient (D_E) gradually increases in early time and reaches its steady limit at a larger time.

II. Increasing the Hartmann number decelerates the radial flow and decreases the value of (D_E). For any value of the Darcy number, the effective dispersion coefficient (D_E) reaches zero when the value of the Hartmann number exceeds 5.

III. An increase in the electro-osmotic Debye–Hückel parameter encourages radial flow; however, the Debye–Hückel parameter shows a dual effect on the effective dispersion coefficient (D_E). For the lower magnitudes of Debye–Hückel parameter, the value of D_E is increased with largerDebye–Hückel parameter; however, at the same time there is an inverse response in D_E for the higher values of Debye–Hückel parameter.

IV. Increasing the first-order chemical reaction parameter weakens the dispersion mechanism, which reduces the values of the effective dispersion coefficient (D_E).

V. Elevation in the Casson viscoplasticparameter helps to increase the effective dispersion coefficient but manifests in a suppression in the peak of the mean concentration.

VI. An increment in the first-order chemical reaction parameter produces a higher peak of the average concentration profile.

VII. The peak of the average concentration tends to be increased for higher magnitudes of Debye–Hückel parameter while it is diminished for lower magnitudes of Debye–Hückel parameter.

The current study has overall revealed some interesting characteristics of hydrodynamic dispersion in reactive non-Newtonian electro-magnetic pulsatile blood flow. However magnetic induction and heat transfer effects have been neglected, which are important in more generalized bioelectromagnetic dispersion transport phenomena [49] and also bio-inspired energy systems [50]. These provide an interesting pathway for future studies as do alternative rheological models e.g., viscoelastic, couple stress [51], micropolar [45], microstretch, etc. Efforts in this direction are currently being explored and will be communicated imminently.

Author Contributions: All the authors contributed to performing the study.

Funding: No funding.

Availability of data and material: Not applicable

Declarations

Conflict of interest: On behalf of all authors, the corresponding author states that there is no conflict of interest.

Appendix. Magnetic and Electric field Expressions

Magnetic field in equation (4) and Poisson- Boltzmann equation (5), which are expressed as follows:

Maxwell's equations are a set of four partial differential equations that describe the force of electromagnetism in an electromagnetic field. The electromagnetic theory depends on Gauss' law, Faraday's law, Ampere's law, and the current continuity equation. These equations are stated mathematically as:

$$\nabla . B_0^* = 0 \tag{A.1}$$

$$\nabla \times E^* = -\frac{\partial B_0^*}{\partial t^*} \tag{A.2}$$

$$\nabla \times M^* = J^* \tag{A.3}$$

$$\nabla . J^* = 0 \tag{A.4}$$

Where B_0^* denotes the magnetic flux, E^* indicates the electric field, M^* represents the magnetic field and J^* designates the current density.

Here $B_0^* = B_1^* + B_2^*$ (Sum of external and induced magnetic field)

Under a small magnetic Reynolds number induced magnetic field $\left(B_2^*\right)$ is negligibly small compared to the external magnetic field $\left(B_1^*\right)$.

Further, the electric field due to the polarization change is also negligible. By Ohm's law

$$J^* = \sigma^* \left(E^* + u^* \times B_0^*\right) \tag{A.5}$$

Where σ^* denotes the electrical conductivity.

The electric fields imposed and induced are presumed to be negligible.

Hence, the term $J^* \times B_0^*$ is simplified as $-\sigma^* B_0^{*2} u^*$

According to the theories of Electrohydrodynamics and Navier-Stokes equations for an incompressible viscous dielectric fluid, the Electrohydrodynamics equations can be summarized as.

$$\nabla . E^* = \frac{\rho_e^*}{\kappa} \quad \left(\text{Gauss law}\right) \tag{A.6}$$

$$E^* = -\nabla \Phi^* \quad \left(\text{Relation between irrotational field and scalar potential}\right). \tag{A.7}$$

$$\nabla . J^* + \frac{\partial \rho_e^*}{\partial t^*} = 0 \tag{A.8}$$

$$\nabla . u^* = 0 \tag{A.9}$$

$$\rho^* \frac{du^*}{dt^*} = -\nabla p^* + \mu^* \nabla^2 u^* + \rho_e^* E_z^* \tag{A.10}$$

Substituting Eqn. (A.7) into Eqn. (A.6), we get the following Poisson's equation

$$\nabla^2 \Phi^* = -\frac{\rho_e^*}{\kappa} \tag{A.11}$$

Where ρ_e^* denotes the net charge density, κ designates the permittivity of the free space (dielectric constant), Φ^* represents the electric potential and E_z^* indicates the component of external electric field applied in the axial direction.

Nomenclature

Symbols	Name	Unit
t^*	Time	s
K^*	Permeability	m^2
$\emptyset$	Porosity	Dimensionless

$\boldsymbol{C}^*$	Solute Concentration	$\mathrm{kg}m^{-3}$
$\boldsymbol{\lambda}^*$	Concentration diffusivity	m^2s^{-1}
$\boldsymbol{k}$	Tortuosity	Dimensionless
$\boldsymbol{D_z^*, D_r^*}$	Axial and transverse diffusion coefficients	m^2s^{-1}
$\boldsymbol{\beta}^*$	Debye–Hückel parameter	m^{-1}
$\boldsymbol{u}^*$	Velocity	ms^{-1}
$\boldsymbol{\Gamma}^*$	Bulk flow reaction rate	s^{-1}
$\boldsymbol{J}^*$	Current density	Cm^{-2}
$\boldsymbol{p}^*$	Superficial pressure including gravity	Nm^{-2}
$\boldsymbol{B}^*$	Total magnetic field	$T(Tesla)$

Table 3. List of variable and parameters

References

1. Taylor, G.I.: Dispersion of soluble matter in solvent flowing slowly through a tube. Proc. R. Soc. London. Ser. A. Math. Phys. Sci. 219, 186–203 (1953)

2. Aris, R.: On the dispersion of a solute in a fluid flowing through a tube. Proc. R. Soc. London. Ser. A. Math. Phys. Sci. 235, 67–77 (1956)

3. Gill, W.-N., Sankarasubramanian, R., Taylor, G.I.: Dispersion of a non-uniform slug in time-dependent flow. Proc. R. Soc. London. A. Math. Phys. Sci. 322, 101–117 (1971)

4. Barton, N.G.: On the method of moments for solute dispersion. J. Fluid Mech. 126, 205–218 (1983)

5. Roy, A.K., Saha, A.K., Debnath, S.: Unsteady convective diffusion with interphase mass transfer in Casson liquid. Period. Polytech. Chem. Eng. 62, 215–223 (2018)

6. Katz, S.: Chemical reactions catalysed on a tube wall. Chem. Eng. Sci. 10, 202–211 (1959)

7. Walker, R.E.: Chemical reaction and diffusion in a catalytic tubular reactor. Phys. Fluids. 4, 1211–1216 (1961)

8. Gupta, P.S., Gupta, A.S.: Effect of homogeneous and heterogeneous reactions on the dispersion of a solute in the laminar flow between two plates. Proc. R. Soc. London. A. Math. Phys. Sci. 330, 59–63 (1972)

9. Shukla, J.B., Parihar, R.S., Rao, B.R.P.: Dispersion in non-Newtonian fluids: Effects of chemical reaction. Rheol. Acta. 18, 740–748 (1979)

10. Kumar, J.P., Umavathi, J.C., Basavaraj, A.: Effects of homogeneous and heterogeneous reactions on the dispersion of a solute for immiscible viscous fluids between two plates. (2012)

11. Roy, A.K., Saha, A.K., Debnath, S.: Hydrodynamic dispersion of solute under homogeneous and heterogeneous reactions. Int. J. Heat Technol. 37, 387 (2019)

12. Roy, A.K., Shaw, S.: Shear augmented microvascular solute transport with a two-phase model: Application in nanoparticle assisted drug delivery. Phys. Fluids. 33, 31904 (2021)

13. Das, P., Mandal, P.K., others: Solute dispersion in Casson fluid flow through a stenosed artery

with absorptive wall. Zeitschrift für Angew. Math. und Phys. 71, 1–24 (2020)

14. Rana, J., Murthy, P.: Solute dispersion in pulsatile Casson fluid flow in a tube with wall absorption. J. Fluid Mech. 793, 877–914 (2016)

15. Rana, J., Murthy, P.: Unsteady solute dispersion in Herschel-Bulkley fluid in a tube with wall absorption. Phys. Fluids. 28, 111903 (2016)

16. Debnath, S., Saha, A.K., Mazumder, B.S., Roy, A.K.: Dispersion phenomena of reactive solute in a pulsatile flow of three-layer liquids. Phys. Fluids. 29, 97107 (2017)

17. Debnath, S., Saha, A.K., Mazumder, B.S., Roy, A.K.: Hydrodynamic dispersion of reactive solute in a Hagen--Poiseuille flow of a layered liquid. Chinese J. Chem. Eng. 25, 862–873 (2017)

18. Debnath, S., Saha, A.K., Siddheshwar, P.G., Roy, A.K.: On dispersion of a reactive solute in a pulsatile flow of a two-fluid model. J. Appl. Fluid Mech. 12, 987–1000 (2019)

19. Debnath, S., Saha, A.K., Mazumder, B.S., Roy, A.K.: On transport of reactive solute in a pulsatile Casson fluid flow through an annulus. Int. J. Comput. Math. 97, 2303–2319 (2020)

20. Chauhan, S.S., Tiwari, A.: Solute dispersion in non-Newtonian fluids flow through small blood vessels: A varying viscosity approach. Eur. J. Mech. 94, 200–211 (2022)

21. Biswas, S., Sarifuddin, Mandal, P.K.: Unsteady transport and two-phase binding of a drug in an atherosclerotic artery. Phys. Fluids. 34, 41905 (2022)

22. Bég, O.A., Bhargava, R., Rawat, S., Halim, K., Takhar, H.S.: Computational modeling of biomagnetic micropolar blood flow and heat transfer in a two-dimensional non-Darcian porous medium. Meccanica. 43, 391–410 (2008)

23. Zhao, M., Wang, S., Wei, S.: Transient electro-osmotic flow of Oldroyd-B fluids in a straight pipe of circular cross section. J. Nonnewton. Fluid Mech. 201, 135–139 (2013)

24. Wang, C., Wong, T.N., Yang, C., Ooi, K.T.: Characterization of electroosmotic flow in rectangular microchannels. Int. J. Heat Mass Transf. 50, 3115–3121 (2007)

25. Bandopadhyay, A., Goswami, P., Chakraborty, S.: Regimes of streaming potential in cylindrical nano-pores in presence of finite sized ions and charge induced thickening: an analytical approach. J. Chem. Phys. 139, 224503 (2013)

26. Misra, J.C., Chandra, S., Herwig, H.: Flow of a micropolar fluid in a micro-channel under the action of an alternating electric field: Estimates of flow in bio-fluidic devices. J. Hydrodyn. 27, 350–358 (2015)

27. Tzirtzilakis, E.E., Loukopoulos, V.C.: Biofluid flow in a channel under the action of a uniform localized magnetic field. Comput. Mech. 36, 360–374 (2005)

28. Sarojamma, G., Ramana, B.: Effect of Magnetic Field on the Dispersion of a Solute in Fluid Flow through a Conduit with Interphase Mass Transfer. In: 2012 Spring Congress on Engineering and Technology. pp. 1–4 (2012)

29. Mazumdar, H.P., Ganguly, U.N., Venkatesan, S.K.: Some effects of a magnetic field on the flow of a newtonian fluid through a circular tube. (1996)

30. Sud, V.K., Sekhon, G.S., Mishra, R.K.: Pumping action on blood by a magnetic field. Bull. Math. Biol. 39, 385–390 (1977)

31. Dash, R.K., Mehta, K.N., Jayaraman, G.: Casson fluid flow in a pipe filled with a homogeneous porous medium. Int. J. Eng. Sci. 34, 1145–1156 (1996)

32. Mehmood, O.U., Mustapha, N., Shafie, S.: Unsteady two-dimensional blood flow in porous

artery with multi-irregular stenoses. Transp. porous media. 92, 259–275 (2012)

33. Dentz, M., Icardi, M., Hidalgo, J.J.: Mechanisms of dispersion in a porous medium. J. Fluid Mech. 841, 851–882 (2018)

34. Shah, P.D., Tiwari, A., Chauhan, S.S.: Solute dispersion in micropolar-Newtonian fluid flowing through porous layered tubes with absorbing walls. Int. Commun. Heat Mass Transf. 119, 104724 (2020)

35. Nakamura, M., Sawada, T.: Numerical study on the flow of a non-Newtonian fluid through an axisymmetric stenosis. (1988)

36. Eldabe, N.T.M., Saddeck, G., El-Sayed, A.F.: Heat transfer of MHD non-Newtonian Casson fluid flow between two rotating cylinders. Mech. Mech. Eng. 5, 237–251 (2001)

37. Roy, A.K., Saha, A.K., Debnath, S.: On dispersion in oscillatory annular flow driven jointly by pressure pulsation and wall oscillation. J. Appl. Fluid Mech. 10, 1487–1500 (2017)

38. Roy, A.K., Saha, A.K., Debnath, S.: Effect of multiple reactions on the transport coefficients in pulsatile flow through an annulus. Int. Commun. Heat Mass Transf. 110, 104369 (2020)

39. Bugliarello, G., Sevilla, J.: Velocity distribution and other characteristics of steady and pulsatile blood flow in fine glass tubes. Biorheology. 7, 85–107 (1970)

40. Masliyah, J.H., Bhattacharjee, S.: Electrokinetic and colloid transport phenomena. John Wiley & Sons (2006)

41. Bég, O.A.: Multi-physical electro-magnetic propulsion fluid dynamics: mathematical modelling and computation. 2–88 (2018)

42. Zeng, L., Chen, G.Q.: Ecological degradation and hydraulic dispersion of contaminant in wetland. Ecol. Modell. 222, 293–300 (2011)

43. Gill, W.-N.: A note on the solution of transient dispersion problems. Proc. R. Soc. London. Ser. A. Math. Phys. Sci. 298, 335–339 (1967)

44. Gill, W.N., Sankarasubramanian, R.: Exact analysis of unsteady convective diffusion. Proc. R. Soc. London. A. Math. Phys. Sci. 316, 341–350 (1970)

45. Roy, A.K., Bég, O.A.: Mathematical modelling of unsteady solute dispersion in two-fluid (micropolar-Newtonian) blood flow with bulk reaction. Int. Commun. Heat Mass Transf. 122, 105169 (2021)

46. Debnath, S., Paul, S., Roy, A.K.: Transport of Reactive Species in Oscillatory Annular Flow. J. Appl. Fluid Mech. 11, (2018)

47. Roy, A.K., Saha, A.K., Ponalagusamy, R., Debnath, S.: Mathematical model on magneto-hydrodynamic dispersion in a porous medium under the influence of bulk chemical reaction. Korea-Australia Rheol. J. 32, 287–299 (2020)

48. Paul, S., Ng, C.-O.: Dispersion in electroosmotic flow generated by oscillatory electric field interacting with oscillatory wall potentials. Microfluid. Nanofluidics. 12, 237–256 (2012)

49. Bég, O.A., Bég, T.A., Munjam, S.R., Jangili, S.: Homotopy and adomian semi-numerical solutions for oscillatory flow of partially ionized dielectric hydrogen gas in a rotating MHD energy generator duct. Int. J. Hydrogen Energy. 46, 17677–17696 (2021)

50. Bég, O.A., Ferdows, M., Shamima, S., Islam, M.N.: Numerical simulation of Marangoni magnetohydrodynamic bio-nanofluid convection from a non-isothermal surface with magnetic induction effects: a bio-nanomaterial manufacturing transport model. J. Mech. Med. Biol. 14, 1450039 (2014)

51. Ponalagusamy, R., Priyadharshini, S.: Couple stress fluid model for pulsatile flow of blood in a porous tapered arterial stenosis under magnetic field and periodic body acceleration. J. Mech. Med. Biol. 17, 1750109 (2017)